Bull Volcanol (2005) 67: 768–782
DOI 10.1007/s00445-005-0433-7

RESEARCH ARTICLE

Agust Gudmundsson · Sonja L. Brenner

On the conditions of sheet injections and eruptions in stratovolcanoes

Received: 12 November 2002 / Accepted: 4 October 2003 / Published online: 1 July 2005

Abstract Nearly all eruptions in stratovolcanoes (composite volcanoes, central volcanoes) are supplied with magma through fractures. Consequently, a primary physical condition for an eruption to occur in a stratovolcano is that a magma-driven fracture is able to propagate to the surface. Magma-filled fractures, frozen or fluid, are referred to as sheet intrusions. More specifically, they are named dykes when subvertical, and inclined (or cone) sheets when inclined. Field observations indicate that most sheet intrusions do not reach the surface to feed eruptions but rather become arrested at various crustal depths. For this reason periods of volcanic unrest with sheet injections are much more common than volcanic eruptions. Whether a sheet intrusion becomes arrested or, alternatively, propagates to the surface depends primarily on the stress field in the stratovolcano. A stratovolcano normally consists of layers of contrasting mechanical properties, such as soft (low Young's modulus) pyroclastic units and stiff (high Young's modulus) lava flows. We present numerical models indicating that volcanoes composed of such layers commonly develop stress fields encouraging sheet and dyke arrest. The models indicate that a necessary condition for a sheet intrusion to reach the surface and feed a volcanic eruption is that the stress field along the sheet pathway becomes homogenised. We propose that much of the activity in a stratovolcano during a volcanic cycle encourages stress-field homogenisation. Field studies show that the sheet intrusions in individual stratovolcanoes have various dips: some are vertical dykes, others inclined sheets, and still others horizontal sills. Analytical models indicate that the dip of a sheet reaching the surface can have great effects on the magma transport during an eruption. This effect is normally greater for a flat volcano such as a collapse caldera than for a stratovolcano that forms a topographic high. We conclude that the shallower the dip of a sheet intrusion, the less will be its volumetric magma transport to the surface of a stratovolcano.

Keywords Volcanic eruption · Sheet arrest · Crustal layering · Crustal stress · Magma transport · Stratovolcano

Communicated by D. Dingwell

A. Gudmundsson (✉) · S. L. Brenner
Department of Structural Geology and Geodynamics,
Geoscience Centre, University of Göttingen,
Goldschmidtstrasse 3,
37077 Göttingen, Germany
e-mail: Agust.Gudmundsson@gwdg.de

Introduction

Why are periods of unrest in stratovolcanoes so much more common than volcanic eruptions? In particular, why do so many sheet intrusions, inferred to be emplaced during periods of unrest, never reach the surface to feed volcanic eruptions? These basic questions in volcanology, although widely recognised, have not been satisfactorily answered. They are clearly related to the physical conditions for the injection of sheet intrusions from the source magma chamber and their propagation to the surface. We believe that these questions need to be answered in order to assess volcanic hazards and, eventually, risks during periods of volcanic unrest.

The answers to these questions must be sought partly in field data on arrested sheet intrusions, and partly in theoretical models to explain these data. Field studies of thousands of sheet intrusions, summarised below, indicate that most become arrested on their way to the surface. Many become arrested in essentially homogeneous and commonly thick layers; others are arrested at contacts between layers (Gudmundsson 2002). Sheet intrusions that end within thick, stiff (high Young's modulus) homogeneous layers, such as many lava flows, thin out to sharp and narrow tips. By contrast, sheet intrusions that end at contacts between layers are thick and have rounded or even blunt tips. Dyke tips in soft (low Young's modulus) layers are also commonly rounded.

Stratovolcanoes consist primarily of lava flows that alternate with beds of pyroclastics, often with weak contacts

between the layers. The lava flows are normally stiff, whereas the pyroclastic layers may be soft (such as young tuff layers) or stiff (such as many welded layers) depending on their age and mode of formation. The models developed below, focusing on abrupt changes in layer stiffness, are thus particularly appropriate for stratovolcanoes. Stratovolcanoes are also referred to as composite or central volcanoes. In this paper, sheet intrusions and sheets are used as generic terms comprising both dykes and inclined (cone) sheets.

For sheet intrusions that eventually reach the surface to feed eruptions in stratovolcanoes, the volumetric rate of magma transport to the surface, an important parameter in assessing volcanic hazards and risks, depends on several factors. The most important parameter is the aperture (opening) which corresponds roughly to the thickness of the sheet intrusion. In some swarms the sheet aperture depends on its dip, with shallow-dipping sheets having smaller apertures (thicknesses) than steep-dipping sheets (Gautneb et al. 1989). In addition, the sheet dip affects the length of the pathway along which the magma is transported to the surface which, in turn, influences the pressure gradient available to drive the magma.

In this paper we explore two main factors that influence the conditions of a volcanic eruption and its volumetric flow rate in a stratovolcano: the local stress field and the dip of the feeder-sheet. Using the results of extensive field observations and analytical and numerical models, we first consider how the local stress field changes with distance from a shallow magma chamber in a volcano consisting of a homogeneous, isotropic rock. Second, we explore the effects that layers with contrasting mechanical properties have on the local stress field in a stratovolcano, and how the local stress field may encourage sheet arrest or sheet propagation to the surface. Third, we provide analytical models of how the dip of a sheet intrusion that reaches the surface of a stratovolcano affects the effusion rate of the resulting eruption.

Arrested sheets

The typical end of a dyke located in a relatively homogeneous, isotropic and stiff material is tapered. For example, in Fig. 1 the dyke gradually decreases in thickness from 0.25 m at the bottom of the exposure to roughly 2 cm at the tip, with no major dyke-generated faults or fractures ahead of the tip.

Figure 2 shows a dyke that ends vertically and bluntly at a sharp contact between a pyroclastic bed and a basaltic lava flow. The dyke thins from 0.38 m at the bottom of the exposure to 0.28 m at its blunt tip where it meets the lava flow. Another example of a dyke tip being arrested at a contact between contrasting lithological types is shown in Fig. 3. This dyke is 0.26 cm thick near the bottom of the exposure, maintaining a similar thickness until just below the contact between a layer of pyroclastic rock and a basaltic lava flow. At the contact, the dyke thins abruptly and ends vertically in the scoracious bottom of the basaltic

Fig. 1 Arrested dyke tip in a vertical section in Tenerife (Canary Islands). The basaltic dyke, hosted by a layer of pyroclastic rock, decreases gradually in thickness from 0.25 m at the bottom of the exposure to ~2 cm at its tip

lava flow. The dyke may continue as an offset segment in a stratigraphically higher pyroclastic layer in the pile, but the segments are not visibly connected through the basaltic lava flow. For comparison, in Iceland dykes are commonly formed by many magma injections, generating separate columnar rows (Gudmundsson 1995a). In some dykes only one injection is able to propagate to the highest level in the layer that eventually arrests the dyke tip.

A clear example of a dyke arrested at a contact is from the Holocene rift zone of the Reykjanes Peninsula in Southwest Iceland (Fig. 4). This dyke, exposed in subvertical sea cliffs, ends only 5 m below the surface of the rift zone. The dyke has a thickness of 0.34 m at the bottom of the exposure but decreases in thickness on approaching the contact between its pyroclastic host rock and the Holocene basaltic flow which forms the surface of the rift zone. The dyke tip is rounded, with no visible faulting or fracturing occurring above it.

These observations indicate that sheet intrusions commonly become arrested when the tips enter layers of high compressive stresses at right angles to the sheet, when the tips meet sharp contacts between mechanically contrasting

Fig. 2 Arrested, blunt dyke tip in a vertical section in Tenerife. This basaltic dyke decreases its thickness by only 10 cm from the bottom of the exposure to the tip, that is, from 0.38 m at the bottom to 0.28 m at the tip. The dyke strikes E–W, is subvertical, and is arrested at the contact, with an attitude of 300/22, between a basaltic lava flow on the top and a pyroclastic rock layer (of scoria and hyaloclastite) below. The notebook provides a scale

Fig. 3 Arrested dyke tip in a vertical section in Tenerife. The basaltic dyke strikes E–W, is subvertical and dissects a pyroclastic rock layer in the lower part of the photograph. The total vertical exposure of the dyke is ~3.7 m. Near the bottom of the exposure, the dyke is 0.26 m thick; it maintains essentially the same thickness up to the contact between the pyroclastic rock and the basaltic lava flow above. There the dyke thins quickly towards its tip. There are no joints or faults at the dyke tip that can be related to stress concentration around the tip

layers, or both. When the tips enter layers of high compressive stress, there is commonly a gradual decrease in the dyke-tip opening (dyke or sheet thickness). By contrast, when the tips reach sharp contacts, the sheets commonly end abruptly with blunt tips.

Sheet dip

Field studies in Iceland and elsewhere indicate that there are commonly two types of swarms of sheet intrusions associated with eroded and extinct stratovolcanoes (central volcanoes). First, there are swarms of regional, subvertical and thick dykes and, second, swarms of local, inclined and thin sheets. Based primarily on data from Iceland and Britain, swarms of inclined sheets associated with extinct, eroded stratovolcanoes are normally circular or slightly elliptical in plan view (Walker 1992; Gudmundsson 1998). On many oceanic islands, dyke complexes have characteristics very similar to those of swarms of inclined sheets (Walker 1992, 1999; Marinoni and Gudmundsson 2000). Many eroded central volcanoes consist largely of inclined sheets.

The following results are thought to be general, but are derived mostly from field observations of extinct stratovolcanoes in Iceland. Most sheets dip towards the source chamber, as represented by a gabbroic pluton, at a depth of 1.5–2 km beneath the initial surface of the volcano. Many sheet swarms show two peaks in the dip distribution, at 75–90° and at 20–50°, but the mean dips in most swarms are between 45° and 65° (Gudmundsson 1995b; Klausen 1999, 2004). The steep-dipping sheets occur mostly in the central part of the swarm, whereas the shallow-dipping sheets are mostly confined to its marginal parts. For example, in a study of 1,128 sheets in a swarm associated with the Therartindur Central Volcano in Southeast Iceland, Klausen (1999) found that the average sheet dip decreases from the central part of the swarm to its marginal parts at the rate of

Fig. 4 Arrested dyke tip in the Holocene rift zone of Southwest Iceland. The dyke is basaltic, strikes NE, is subvertical, and dissects pyroclastic rock (volcanic tuff) in the lower part of the photograph. The dyke thins gradually from 0.34 m at the bottom of the 8 m tall exposure to 0.1 m at its tip. The tip is arrested at the contact between the pyroclastic rock and the Holocene basaltic lava flow that forms the surface of the rift zone. There is no dyke-related faulting or fracturing above the dyke tip

$\sim$16° per kilometre. Sheet dip in Iceland is steeper than that in the British Isles, with an average dip of $\sim$45° (Billings 1972; Hills 1972), and Gran Canaria (Canary Islands), with an average of $\sim$41° (Schirnick et al. 1999). However, there exist individual sheet swarms in Iceland with average dips of only 34° (Gudmundsson et al. 1996).

In the Icelandic swarms, the sheets range in thickness from a few centimetres to 14 m. The average sheet thickness in individual swarms ranges from 0.1 m (Gudmundsson et al. 1996) to around 1 m. For example, for 1,128 sheets in the Thverartindur Central Volcano, Klausen (1999, 2004) obtained an average thickness of around 0.9 m. Commonly, the statistical thickness size distribution follows approximately a power law or some other law with a negative exponent (Klausen 1999). In Icelandic stratovolcanoes sheet thicknesses are generally similar to those in many ophiolites (Pallister 1981) and oceanic islands (Walker 1992, 1999; Marinoni and Gudmundsson 2000).

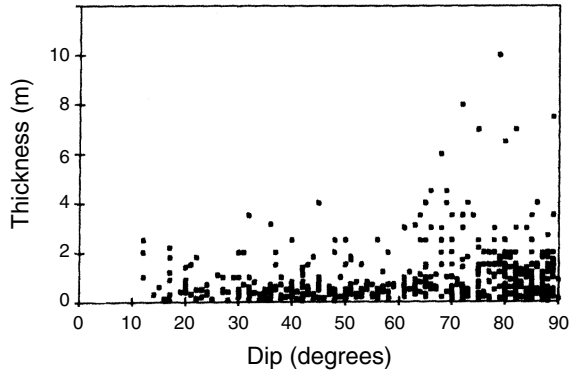

Fig. 5 Dip versus thickness (aperture) of 504 inclined sheets in the extinct Tertiary stratovolcano of Hafnarfjall in West Iceland (Gautneb et al. 1989; Gudmundsson 1995b). Only sheets that are steeply dipping (>70°) reach great thicknesses (>4 m)

Fig. 6 Part of a swarm of inclined (cone) sheets in the Geitafell Volcano, an extinct and deeply eroded Tertiary stratovolcano in Southeast Iceland (located in Gudmundsson 1995b, 1998). View west, in the lower part of the photograph, 80–90% of the rock consists of inclined sheets, mostly 0.5–1 m thick, whereas in the upper part of the photograph there is a gabbro pluton. This pluton marks the uppermost part of the extinct shallow chamber that supplied magma to the inclined sheets when the volcano was active

In some swarms shallow-dipping sheets are thinner than steep-dipping sheets (Fig. 5). This indicates that, while they are fluid-filled fractures, shallow-dipping sheets have commonly smaller apertures and lower volumetric flow rates than steep-dipping sheets.

In the vicinity of the gabbro plutons that represent tops of extinct chambers the entire rock may be composed of sheets (Fig. 6). However, the intensity of sheets, defined as number of sheets per unit length of profile, falls off rapidly with distance from the margin of the pluton. This fall-off in intensity is partly related to the increase in the cross-sectional areas of crustal "shells" that the sheets dissect with increasing distance from the pluton (Fig. 7). Partly, however, the fall-off results from many sheets becoming arrested at short distances from the pluton and, therefore, never reaching the surface to feed volcanic eruptions.

Cross-cutting relationships between most sheets indicate that the only displacement on the earlier sheet is

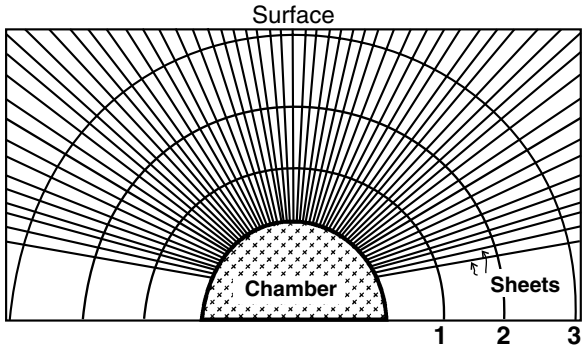

Fig. 7 One reason why the intensity of sheets (measured as number of sheets dissecting unit length of a profile) falls off with distance from the source magma chamber is that the sheets dissect progressively larger cross-sectional areas (half-circles 1–3). However, because the perimeter of a circle ($2\pi r$) increases directly with its radius r, and the surface area of a spherical shell ($4\pi r^2$) is a function of the radius squared, it follows that the abrupt decrease in intensity with distance from the source chamber can only be partly explained by an increase in area through which the sheets pass. We propose that the main reason for fall-off in sheet intensity with distance from the chamber is that most of the sheets become arrested at short distances from their sources

opening perpendicular to the trend of the later sheet (Gudmundsson 2002). These observations suggest that most sheets form their (often irregular) pathways not as shear fractures (faults), but rather as magma-driven extension (mode I) fractures.

Models of sheet arrest

We explore the conditions for sheet arrest using two types of models: analytical and numerical. The analytical models are only applicable where the crust hosting the source magma chamber of the stratovolcano can be assumed homogeneous and isotropic. This is rarely a viable assumption, particularly in young stratovolcanoes with numerous layers of contrasting mechanical properties and weak contacts in between. Here a "weak contact" means one with low tensile strength and shear strength. Thus, in this model section the focus will be on numerical models where the mechanical heterogeneity and anisotropy, through layering, can be taken into account. We begin the section, however, by a brief review of the stress field around a spherical magma chamber in a homogeneous, isotropic crust.

Homogeneous and isotropic crust

Field and theoretical considerations indicate that some shallow crustal magma chambers may be nearly spherical in shape (Gudmundsson 1998). Active magma chambers are also commonly modelled as spherical (Mogi 1958; McTigue 1987; Delaney and McTigue 1994). We can thus approximate a shallow chamber as a sphere of radius R_1 and take the outer radius of the elastic body within which the chamber is located (here, a crustal segment) as R_2, where $R_2 \gg R_1$. The chamber is subject to internal total fluid pressure P_t at its radius R_1, whereas the crustal segment is subject to lithostatic stress p_l at the outer radius R_2 (Gudmundsson 2002). In this model, we effectively assume that $R_2 \rightarrow \infty$, which means that the free-surface effects are not taken into account. The shallow chamber must therefore be at a crustal depth much larger than its radius.

Using spherical polar coordinates (r, θ, φ), where r is the radius vector, θ is the angle between the radius vector and a fixed axis, and φ is the angle measured around this axis, the radial stress σ_r becomes (Saada 1983):

$$\sigma_r = P_t \left(\frac{R_1}{r}\right)^3 + p_l \left[1 - \left(\frac{R_1}{r}\right)^3\right] \quad (1)$$

where P_t is the total fluid pressure in the chamber, and p_l is the lithostatic stress or pressure at the depth of the chamber. Because of spherical symmetry, the stresses σ_θ and σ_ϕ are equal and given by:

$$\sigma_\theta = \sigma_\phi = -\frac{P_t}{2}\left(\frac{R_1}{r}\right)^3 + \frac{p_l}{2}\left[\left(\frac{R_1}{r}\right)^3 + 2\right] \quad (2)$$

A magma-filled chamber ruptures and initiates a sheet intrusion when the following conditions are satisfied:

$$P_t = \sigma_3 + T_0 \quad (3)$$

or

$$p_l + p_e = \sigma_3 + T_0 \quad (4)$$

Here, $p_e = P_t - p_l$ is the excess magmatic pressure in the chamber, that is, the difference between the total magma pressure, P_t, in the chamber when it ruptures and the lithostatic stress p_l. Because sheet intrusions are mostly extension fractures, they form in a direction that is perpendicular to the minimum principal stress σ_3. Thus, for a sheet intrusion to occur, the excess pressure in the chamber must reach the local in situ tensile strength, T_0, of the chamber walls at the site of rupture. Compressive stress is considered positive so that for absolute tension σ_3 is negative, whereas the maximum compressive principal stress, σ_1, is always positive.

If the excess magma pressure p_e, as defined above, is used instead of the total pressure P_t, Eqs. (1) and (2) simplify to:

$$\sigma_r = p_e \left(\frac{R_1}{r}\right)^3 \quad (5)$$

$$\sigma_\theta = \sigma_\phi = -\frac{p_e}{2}\left(\frac{R_1}{r}\right)^3 \quad (6)$$

showing that the intensity of the stress field associated with a spherical magma chamber falls off inversely as the cube

of the distance r from the chamber (Gudmundsson 2002, Fig. 14). The excess pressure p_e is normally equal to the local tensile strength at the time of chamber rupture and sheet intrusion [Eqs. (3) and (4)]. In situ tensile strengths of rocks are generally very low, typical values being 0.5–6 MPa (Haimson and Rummel 1982; Schultz 1995; Amadei and Stephansson 1997). Consequently, at chamber rupture and initiation of a sheet intrusion, the tensile stresses at the margin of the chamber are small and decrease rapidly with distance along the potential pathway of the propagating sheet intrusion.

These results indicate that the stress conditions for sheet intrusion and propagation may commonly be satisfied in the vicinity of a magma chamber while, at a certain distance from the chamber, conditions for sheet arrest are satisfied. This implies that many sheet intrusions propagate for only a short distance from the chamber until they enter a layer, or a "shell", where the stress conditions are unfavourable for their propagation (a stress barrier) and they become arrested (Gudmundsson 2002; this paper).

These results agree with those obtained in numerical models of a magma chamber with a circular cross section in a homogeneous, isotropic crust, using the BEASY (1991) boundary element program (Fig. 8). The details of the boundary-element method in general, and that of the BEASY program in particular, are provided by Brebbia and Dominguez (1992), the BEASY homepage (http://www.beasy.com), BEASY (1991), and Jing and Hudson (2002). Here we use the BEASY program also for the models in Figs. 9–13. In all the numerical models, the upper surface (marked as surface in some of the models) is a free surface.

The model in Fig. 8 is of unit height (vertical dimension) and width (horizontal dimension). All other dimensions are fractions of these units. A magma chamber of a circular cross section, with a diameter of 0.25 units, is located in the centre of the model, so that the top and bottom of the chamber are at distances of 0.375 units from the upper and lower edge of the model. The magma chamber is located in a crust with a uniform Young's modulus (stiffness) of 10 GPa, and a Poisson's ratio of 0.25. These values correspond to those of many sedimentary rocks in the uppermost part of the crust (Bell 2000). The only loading in the model is a magmatic excess pressure [defined in Eq. (4)] of 10 MPa in the chamber. In solid mechanics, "load" is a generic word used mostly to denote the forces, stresses, or pressures that are applied to a body and external to its material (Benham et al. 1996). Here, "loading" denotes the fluid pressure, the stress, or both used in the numerical models. To avoid rigid body rotation and translation, the model is fastened in all the corners.

The results show that the highest tensile stresses occur at the walls of the magma chamber and fall off rapidly with distance from the chamber. These results agree with those from earlier analytical and numerical studies (Savin 1961; Gudmundsson 1998); they indicate that the intensity of a sheet swarm injected from a chamber subjected to magmatic excess pressure as the only loading decreases markedly away from the margins of the chamber. This result

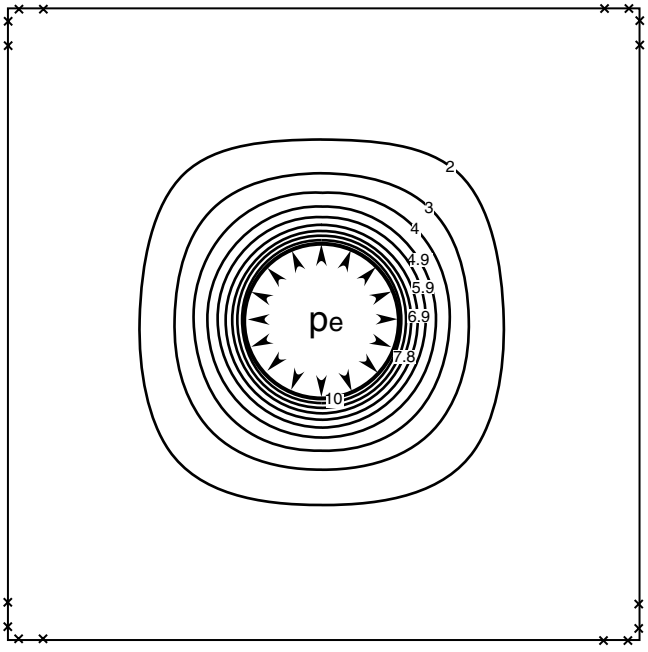

Fig. 8 Boundary-element results showing the concentration of the maximum principal tensile stress (minimum principal compressive stress) σ_3, in mega-pascals, around a magma chamber of circular cross section subject to internal magmatic excess pressure, p_e, of 10 MPa as the only loading. The reason why the σ_3-contours approach a square shape with increasing distance from the chamber (also see Figs. 9 and 10) is due to the square shape of the modelled elastic plate. The chamber is located in a homogeneous and isotropic crust with a Young's modulus of 10 GPa, similar to that of many pyroclastic and sedimentary rocks (Bell 2000). The *crosses* indicate the boundary conditions of no displacement in the model. In this model the diameter of the chamber is 0.25 units, whereas the height of the model is one unit. Thus, in a crust of thickness 10 km, the chamber diameter would be 2.5 km, and the depth of the top of the chamber below the free surface would be 3.75 km. The maximum tensile stress concentration occurs at the margins of the chamber and decreases rapidly with distance from the chamber [cf. Eqs. (5) and (6)]

is in general agreement with that observed in many sheet swarms (Anderson 1936; Billings 1972; Schirnick et al. 1999; Gudmundsson 2002; Klausen 2004).

Layered crust

The results from the last section apply if the host rock of the chamber is homogeneous and isotropic whereas, normally, the rock is heterogeneous and (often highly) anisotropic. In particular, layering and weak contacts in the host rock may encourage significant variations in the stress field that can contribute to the arrest of sheet intrusions.

The model in Figs. 9 and 10 is the same as in Fig. 8 except that the crust now consists of layers A–D with different Young's moduli (stiffnesses). Again, the model (Figs. 9 and 10) is of a unit height (vertical dimension) and all layer thicknesses are given as fractions of this unit. Each of layers A, B and C has a thickness of 0.1 unit. As in Fig. 8, the magma chamber has a diameter of 0.25 units and is located in the model centre, so that its top and bottom are

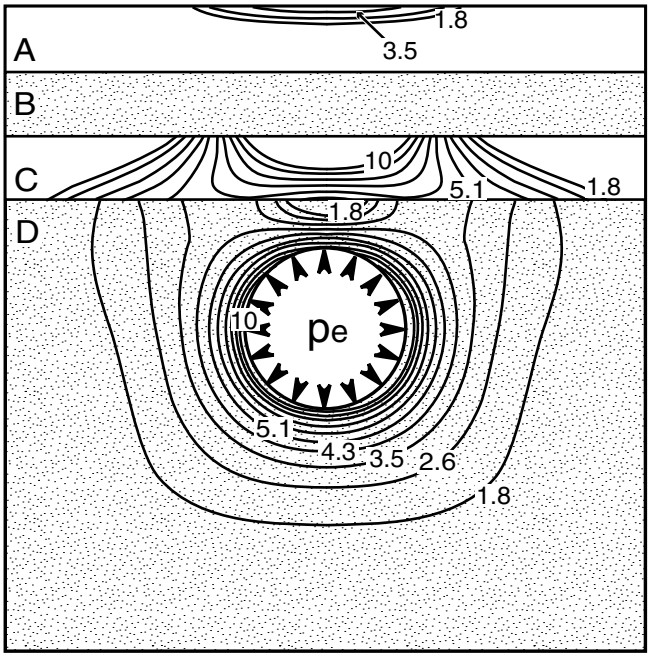

Fig. 9 Boundary-element results showing the concentration of the maximum principal tensile stress (minimum principal compressive stress) σ_3, in mega-pascals, around a magma chamber of circular cross section subject to internal magmatic excess pressure, p_e, of 10 MPa as the only loading. The geometry, chamber size and loading are the same as in the model in Fig. 8, but here the chamber is located in a layered crust where each layer (except D) has a thickness of 0.1 unit. Layer D has a stiffness of 10 GPa, layer C 100 GPa, layer B 1 GPa, and layer A 100 GPa

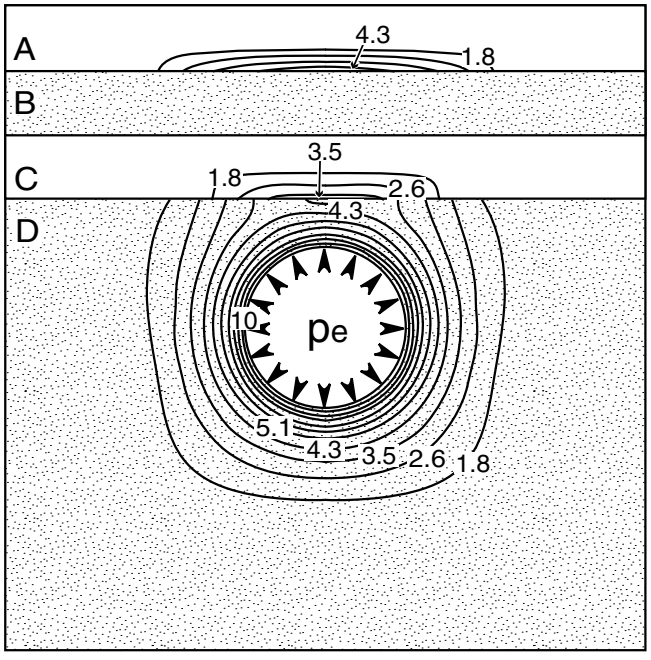

Fig. 10 Boundary-element results showing the concentration of the maximum principal compressive stress (minimum principal tensile stress) σ_1, in mega-pascals, around a magma chamber, of circular cross section subject to internal magmatic excess pressure, p_e, of 10 MPa as the only loading. This is the same model as in Fig. 9

at 0.375 units from the upper and lower surfaces of the model. For example, if the chamber were located in a crust with a thickness of 10 km, the diameter of the chamber would be 2.5 km, the depth of its top below the free surface of the associated volcano would be 3.75 km, and each of the layers A, B and C would be 1 km thick.

Layer D has the same stiffness (10 GPa) as in Fig. 8, whereas the stiffness of layer A is 100 GPa, layer B 1 GPa, and layer C 100 GPa. Such extreme variations in stiffness may not be very common in the crust. However, they underline the large effects that contrasts in Young's modulus can have on the local stress fields within stratovolcanoes, and the potential effects of these stress fields on sheet arrest. Furthermore, these stiffness values correspond to the range for common bedrocks, 1–100 GPa, as measured in the laboratory (Afrouz 1992; Bell 2000). In stratovolcanoes, some rock layers may exceed this range. For example, layers of basalt and gabbro may reach stiffnesses of 110–130 GPa, whereas layers of volcanic tuffs and other pyroclastic rocks may have stiffnesses of as little as 0.1 GPa and, occasionally, 0.05 GPa (Bell 2000). The range of Poisson's ratios for bedrocks is normally much narrower. For example, 0.25 is a typical Poisson's ratio for many basalts and soft pyroclastic rocks (Bell 2000); this value is used in all the numerical models in this paper.

In situ elastic properties are normally different from those measured in the laboratory. In particular, the in situ stiffness of a rock mass tends to be considerably less than that measured of the same rock type in the laboratory because of the numerous pores, fractures and other discontinuities in the rock mass that lower its stiffness (Goodman 1989; Priest 1993). The differences between the laboratory and in situ values, however, decrease with increasing pressure and temperature, and thus with increasing depth in the crust. Based on these considerations, we take 1–100 GPa as a reasonable range in stiffnesses of layers in a mature stratovolcano.

In the model (Figs. 9 and 10), the surface layer A, as well as the third layer C, are very stiff (100 GPa) whereas layer B is very soft (1 GPa) and layer D, where the chamber is located, is relatively soft (10 GPa). For an active stratovolcano, layers A and C could thus represent stiff basaltic or intermediate lava flows, or sills, and layer B soft tuff. Layer D, hosting the chamber, could represent sedimentary rocks. The results (Fig. 9) show that the maximum principal tensile stress, σ_3, is concentrated at the upper margins of the walls (perimeter) of the chamber, suggesting that the highest intensity of sheet intrusion would be in these areas. The results (Fig. 9) also show that tensile stresses concentrate in the stiff layers A and C, in particular in the upper parts of these layers. These stresses are shown by the contours of the maximum tensile (minimum compressive) principal stress σ_3. By contrast, the maximum principal compressive stress, σ_1, is concentrated in the lower parts of these same layers (Fig. 10). The principal stresses σ_1 and σ_3 are, by definition, at right angles to each other. The results presented in Figs. 9 and 10 show only the magnitudes, but not the directions, of these principal stresses. It follows that there may be tension and compression at the same sites

in the model, but in directions that differ by 90° (Figs. 9 and 10).

The contours of the principal stress magnitudes presented in Figs. 9 and 10 suggest that the effects of inflation of a magma chamber located in the layered crust of a stratovolcano may be similar to convex bending of a layered plate. Thus, the stiff layers become subject to tensile stresses in their upper parts, above the neutral surface, and compressive stresses in their lower parts, below the neutral surface. Subvertical sheet intrusion would then be encouraged in the upper parts of the stiff layers, but sheet arrest in the lower parts. In the absence of sheet injection, the conditions in the upper parts of layers A and C during magma-chamber inflation would be favourable for normal faulting.

The results also indicate that there are essentially no stress concentrations in the soft layer B (Figs. 9 and 10). This layer would therefore be expected to act as a stress barrier to subvertical sheet propagation from the magma chamber. Also, if normal faulting were to occur in the upper part of layer C, layer B would tend to arrest the upward propagation of the faults. Thus, a soft layer such as B may be a barrier to the propagation of sheet intrusions and, temporarily, prevent them from reaching the surface to feed eruptions.

Sheet geometry in a layered crust

Strong contrasts in the mechanical properties of a layered crust of a stratovolcano contribute to the arrest of sheet intrusions and affect the geometry of the arrested sheets. Here we focus on the tip geometries of arrested vertical sheet intrusions, that is, dykes, using the configuration in Fig. 11 to obtain the results in the models in Figs. 12 and 13.

In both models, there is a linear variation in the magmatic overpressure, P_0, from the centre of the dyke at the bottom of the model to its tip (Fig. 11). A slight downward bending of the surface that occurs in some models is not shown. The magmatic overpressure (also referred to as driving pressure or net pressure) is here defined as the total magma pressure P_t minus the minimum compressive principal stress σ_3, that is, $P_0 = P_t - \sigma_3$. Here the contrast in stiffness is smaller than that in the boundary-element models above (Figs. 8–10) so as to emphasise the sensitivity of the dyke shape to moderate changes in Young's modulus of the host rock. Thus, the stiffest layer has a Young's modulus of 100 GPa, the same as in the model above (Figs. 9 and 10), the intermediate-stiff layer a Young's modulus of 40 GPa, and the softest layer has a Young's modulus of 4 GPa.

The dyke is supposed to be arrested on entering a stress barrier. It follows that the uppermost layer is subject to a horizontal compressive stress, which is here taken as 10 MPa. This is similar to the additional horizontal compressive stresses found in some stress barriers in the palaeorift zones of Iceland (Haimson and Rummel 1982). There are various ways by which such stress barriers develop (Gudmundsson 2002). In this case, the uppermost layer could have become a stress barrier as a result of horizontal compressive stresses generated by earlier dykes that dissect

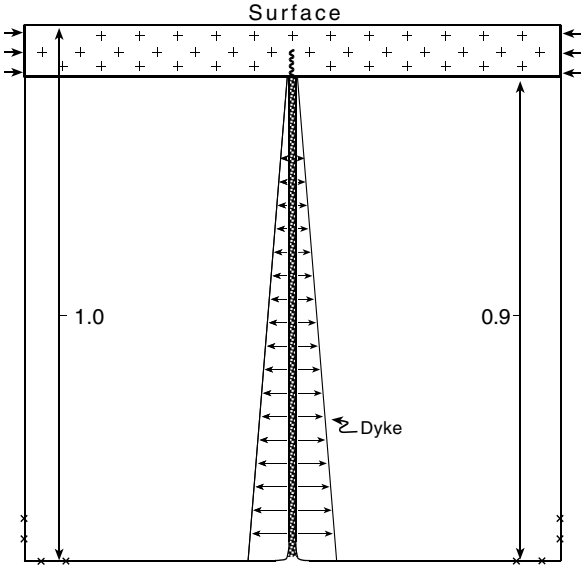

Fig. 11 Illustration of the boundary element model used for the calculations presented in Figs. 12 and 13. A hydrofracture (e.g., a dyke) is subject to an internal fluid overpressure that varies from 10 MPa at its bottom to 0 MPa at its tip, where it meets with a surface layer subject to 10 MPa horizontal compressive stress (as indicated by the *arrows*). This horizontal compressive stress may be partly due to gravity, to some tectonic stress (e.g., related to earlier feeder dykes or normal faulting in a rift zone), or both. Here this compressive stress is presented as an average for the whole layer. The lower half of the surface layer has a vertical weakness which is presented by an internal spring (thick, sinuous line) of stiffness 6 MPa m^{-1}. The model has unit dimensions, the tip of the hydrofracture being at a depth of 0.1 unit below the free surface. For example, if the hydrofracture is a dyke coming from a magma reservoir with 10 MPa overpressure at 10 km depth, the tip of the dyke would be at 1 km depth below the free surface. Poisson's ratio of all layers is 0.25; Young's modulus varies

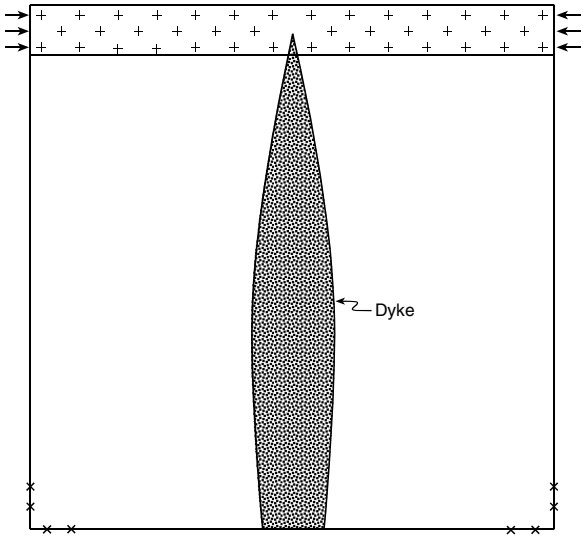

Fig. 12 Boundary-element results showing the shape of the dyke in Fig. 11 when the surface layer is stiffer (that is, has a higher Young's modulus, E) than the rest of the host rock. Here the surface layer has E=100 GPa, whereas the rest of the host rock has E=40 GPa, the latter value being typical for the upper part of the crust in Iceland

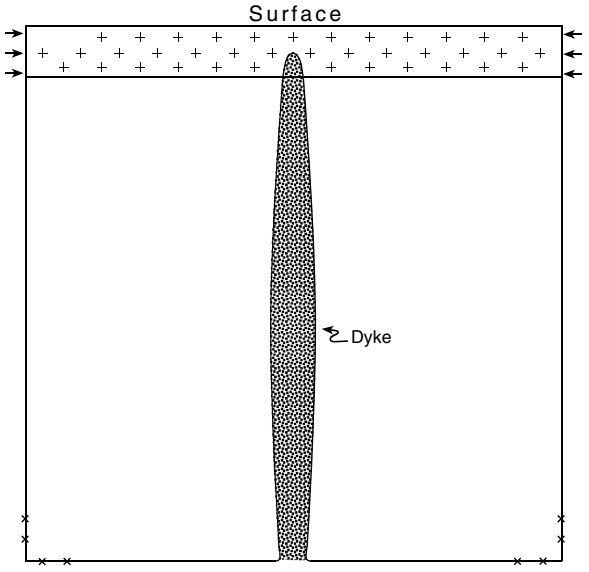

Fig. 13 Boundary-element results on the shape of the dyke in Fig. 11 when the surface layer is softer (that is, has a lower Young's modulus) than the rest of the host rock. Here the surface layer has E=4 GPa, whereas the rest of the host rock has E=40 GPa

the layer, by normal faulting in that layer, or by bending of the layer.

The results (Figs. 12 and 13) show that the resulting shape of a dyke whose tip enters a soft layer is very different from that of a dyke that meets a stiff layer. In Fig. 12, Young's modulus is higher (100 GPa) in the upper layer than in the lower layer (40 GPa), whereas in Fig. 13 Young's modulus is lower (4 GPa) in the upper layer than in the lower layer (40 GPa).

These models indicate that when the dyke enters a soft layer its tip becomes rounded and relatively wide, but with a small region of tensile stress concentration, whereas the rest of the dyke becomes relatively thin (Fig. 13). By contrast, when the dyke enters a stiff layer its tip becomes narrow and sharp, with a large area of high tensile stress concentration, whereas the rest of the dyke becomes relatively thick (Fig. 12). These model results are supported by field observations of dyke tips (Gudmundsson 2002).

Models of sheet dip

Sheet dip depends on the loading of the source magma chamber. An active magma chamber that ruptures to inject sheets must be subject to an internal fluid excess pressure $p_e = P_t - p_l$ that is so high as to satisfy Eq. (4) . The loading conditions by which Eq. (4) is satisfied, however, may vary (Gudmundsson 1998). In some cases, magma volume is added to the chamber until it reaches the conditions of Eqs. (3) and (4). In other cases, particularly at divergent plate boundaries, it is an external absolute or relative tensile stress related to plate pull that brings the fluid pressure in the chamber to the conditions of rupture [Eqs. (3) and (4)].

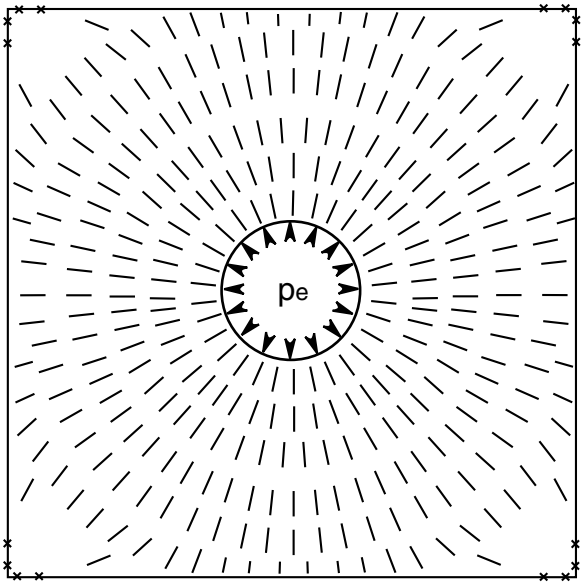

Fig. 14 Finite-element results on the stress field around a magma chamber of circular vertical cross-section subject to internal magmatic excess pressure p_e=10 MPa. The *ticks* represent the direction (trajectories) of the maximum principal compressive stress, σ_1, along which ideal sheet intrusions from the chamber would propagate. The model is similar to that in Fig. 8. The *crosses* indicate the boundary conditions of no displacement in the model

Homogeneous, isotropic crust

The trajectories of the maximum principal compressive stress, σ_1, represent the ideal pathways along which sheet intrusions injected from a chamber will propagate (Gudmundsson 1998). Stress trajectories are obtained directly from the ANSYS finite element program, which is used for the models in Figs. 14 and 15. The details of the finite-element method in general, and that of ANSYS in particular, are provided by Zienkiewicz (1977), Logan (2002), and the ANSYS homepage (http://www.ansys.com). A general review of the various numerical methods applied to rock-mechanics problems, including the finite and boundary element methods used here, is given by Jing and Hudson (2002).

In the model in Fig. 14, the only loading is the 10 MPa magmatic excess pressure in the chamber. This is thus a similar model to the boundary-element model in Fig. 8. The stress field, as presented by the stress trajectories (ticks), depends on the loading conditions. If the loading conditions are different, the sheet dip is likely to be different from that in Fig. 14, even if the crust is still considered homogeneous and isotropic. For example, the trajectories of σ_1 are, on average, shallower when the only loading is internal fluid excess pressure in the absence of external tension (Fig. 14) than when the loading includes an external horizontal tension (Gudmundsson 1998, 2002).

These different loading conditions of shallow magma chambers may partly explain the difference in the average dip of sheet swarms in Iceland as compared with the British Isles and Gran Canaria. It was noted earlier that the most

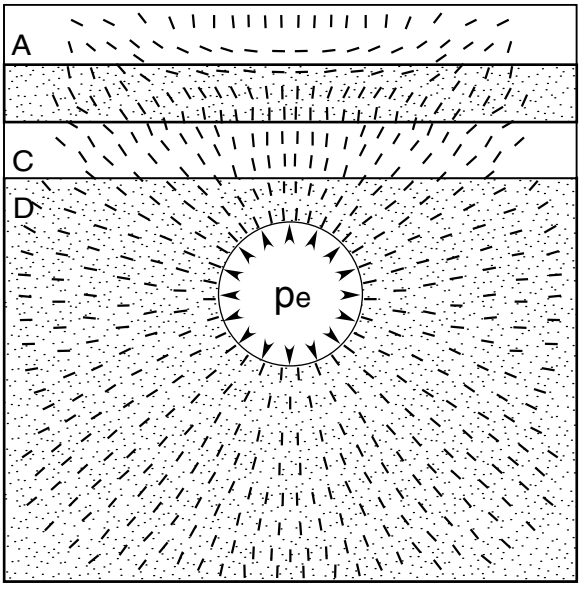

Fig. 15 Finite-element results on the stress field around a magma chamber of circular vertical cross-section subject to internal magmatic excess pressure p_e=10 MPa. The *ticks* represent the direction (trajectories) of the maximum principal compressive stress, σ_1, along which ideal sheet intrusions from the chamber would propagate. The model is the same as that in Figs. 9 and 10

common dips of sheets in Icelandic central volcanoes are between 45° and 65°, whereas the average dip in the British sheet swarms is around ~45° (Billings 1972; Hills 1972) and that in Gran Canaria ~41° (Schirnick et al. 1999). Being at divergent plate boundaries, magma chambers that give rise to sheet swarms in Iceland are likely to be subject to an external absolute or relative tensile stress, in addition to the internal magma pressure that derives from magma being added to the chamber. By contrast, the magma chambers that gave rise to the sheets of the British Isles and Gran Canaria were not associated with divergent plate boundaries and were, presumably, subject to internal fluid excess pressure as the principal or sole loading.

A simple model of a chamber in a homogeneous, isotropic crust (Fig. 14) may give a reasonable explanation of the general dip distribution in many swarms. Different sheet dips, however, are to be expected during the evolution of the swarm. One reason is that the stress field, and thus the pattern of stress trajectories, changes when the geometry of the source chamber changes (Gudmundsson 1998). A second reason is that crustal anisotropy and heterogeneity, particularly layering, may have significant effects on the local stress field.

Layered crust

For a layered crust, the trajectories of the maximum principal compressive stress, σ_1, around a magma chamber may be very different from those of a chamber in a homogeneous crust. Figure 15 shows the stress trajectories for the model of a magma chamber in a layered crust as presented in Figs. 9 and 10. There is a change in the dip of the σ_1- trajectories at the contact between the stiff layer C (100 GPa) and the relatively soft layer D (10 GPa) which hosts the chamber. However, the most significant dip changes occur in layers B and A and, particularly, at the contact between these layers where the trend of σ_1 is horizontal directly above the magma chamber.

The effects of the changes in the dip of σ_1 on the potential sheet pathways are best discussed with reference to Figs. 9 and 10 in addition to Fig. 15. Based on the results in Figs. 9 and 15, for the given loading conditions, sheet intrusions will normally be able to propagate from the chamber and up into layer C. Depending on the point of rupture and sheet injection at the chamber walls, the sheet intrusion will either be subvertical or inclined and decrease in dip with increasing depth of injection along the chamber walls. The results in Fig. 9 show no tensile stress concentration in layer B, suggesting that this layer will normally act as a stress barrier to sheet propagation. The results in Fig. 15, however, indicate that if a sheet is able to propagate into layer B it will be subvertical in the lower part of the layer, but tend to stop or become subhorizontal in the upper part of that layer.

The results in Fig. 15 show that the maximum principal stress σ_1 is horizontal at the contact between layers B and A and, in particular, in the lower part of the surface layer A. Figure 10 shows no compressive stress concentration in layer B, but in excess of 4 MPa in the lower part of layer A. This concentration of horizontal compressive stress in the lower part of layer A indicates that it will normally act as a stress barrier to the propagation of subvertical or inclined sheet intrusions from the magma chamber below. Thus, for the given loading conditions and mechanical properties of the layers, many, and perhaps most, sheet intrusions not already arrested in layer B would become arrested in the lower part of the surface layer A. Gradual stress-homogenisation of the layers, however, would eventually allow one or more sheet intrusions to reach the surface so as to supply magma to an eruption. Then, however, the aperture and dip of the feeder sheet would be among the most important factors controlling its volumetric flow rate of magma.

Magma flow in feeder dykes—theory

The analytical and numerical results above indicate that stress fields around magma chambers commonly favour sheet injection in a shell surrounding the chamber while sheet and dyke arrest is favoured at greater distances from the chamber (Fig. 16). Because the sheets are subject to magmatic overpressure (Gudmundsson 2002), on injection from a magma chamber they relax the absolute and relative tensile stresses in the vicinity of the chamber. When tensile stresses build up repeatedly at the chamber, by external loading such as plate pull or adding magma to the chamber, the sheet intrusions injected from the chamber homogenise the stress field in shells or layers of gradually larger radius vectors around the chamber (Fig. 16). Thus, the host rock volume around the chamber into which sheet intrusions

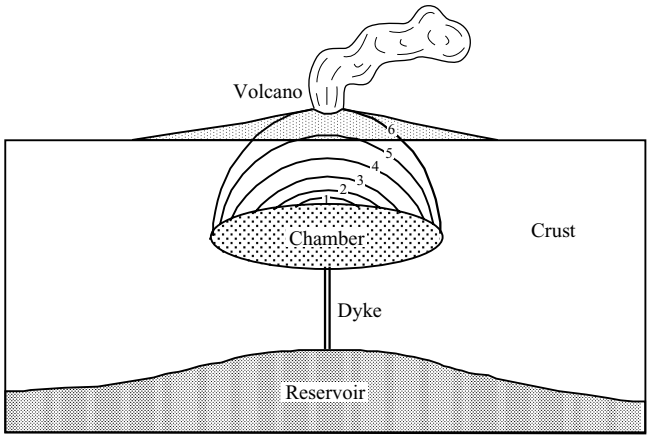

Fig. 16 Most sheet intrusions from the shallow magma chamber in the stratovolcano become arrested in various crustal shells or barriers (1–5) where the stresses are unfavourable for sheet propagation. The sheet injections, however, gradually homogenise the stress field to the surface (6), at which stage one or more eruptions may occur. The average time between successive eruptions in a stratovolcano is referred to as a stress (or volcanic) cycle (cf. Gudmundsson 2002). Stratovolcanoes are commonly supplied with magma through a double chamber where a deep-seated reservoir supplies primitive magma to a shallow chamber

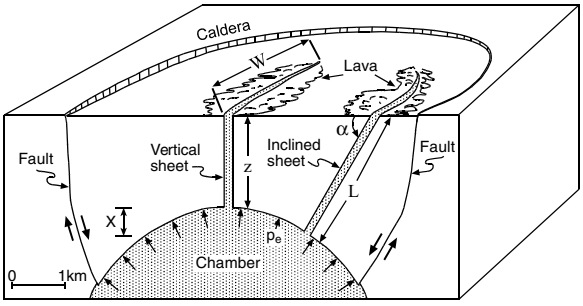

Fig. 17 Volumetric magma flow through a sheet to the surface in a stratovolcano (here, a collapse caldera) depends on the dip of the sheet. A vertical sheet has a dip dimension z, whereas an inclined sheet dipping α has a dip dimension L; for both sheets the width (the outcrop length) in a direction perpendicular to the magma flow is W. The excess magmatic pressure in the chamber is p_e, and the difference in depth between the point of initiation of the vertical and the inclined sheet is denoted by x (Eq. (12))

can propagate, for a given size and loading of the chamber, gradually increases with time (Fig. 16).

This homogenisation of the stress field by means of injection of sheet intrusions occurs also if the host rock is layered and anisotropic. A sheet intrusion, of given overpressure (as the only loading) and dimensions, that propagates through a soft layer becomes thick, but thin when it propagates through a stiff layer (Bonafede and Rivalta 1999; Brenner and Gudmundsson 2002). The different compressive stresses generated by sheet intrusions when passing through different layers contribute to a gradual homogenisation of the local stress field within the stratovolcano. When the conditions presented in Eqs. (3) and (4) are satisfied in the host rock to the surface in a part of the stratovolcano, a sheet intrusion may propagate to the surface and supply magma to a volcanic eruption (Fig. 17). At this stage, the stress field has been homogenised along the pathway of the sheet intrusion to the surface. The feeder sheets (Fig. 17), however, normally bring the state of stress back to one similar to that existing at the beginning of the stress cycle, which thereby may be re-initiated. Each stress (or volcanic) cycle is normally roughly equal in length to the average time between volcanic eruptions, which in Iceland is commonly a few hundred years (Gudmundsson 1998, 2002). This model implies that during most periods of unrest resulting in sheet intrusion from a magma chamber of a volcano, there will be no volcanic eruptions, a conclusion which is supported by the abundant occurrence of arrested sheet intrusions.

Although there are many analytical solutions for the flow of magma in idealised dykes in an isotropic, homogeneous crust (Spence et al. 1987; Lister and Keer 1991; Rubin 1995), there exist no analytical solutions concerning the details of the propagation of a sheet intrusion through anisotropic, jointed and layered rocks with numerous sharp contacts, stress barriers and changes in elastic properties. Here we examine only fluid flow in sheet intrusions that reach the surface in an active stratovolcano or a caldera. As is indicated in Figs. 5–7, 14, and 15, the attitude of these intrusions can range from vertical to horizontal; we focus mainly on the effect of their dips on the overpressure and volumetric flow rate.

We analyse the flow of magma through a sheet intrusion in a host rock that is assumed to behave as rigid and, alternatively, as elastic. These assumptions are frequently made when considering the flow of fluids in the crust. For a rigid host rock, we refer to the resulting magma-filled fractures (and the source chamber) as self-supporting, using the superscript s for the volumetric flow of magma through the fracture. Alternatively, if the magma-filled fractures (and chamber) deform as the magma pressure changes, the fracture is referred to as elastic, using the superscript e for the volumetric flow of magma through the fracture.

Consider first a vertical, self-supporting magma-filled fracture that extends from its source chamber to the surface of a volcano (Fig. 17). From the Navier-Stokes equations (Lamb 1932; Milne-Thompson 1996) it follows that the volumetric flow rate, Q_z^s , through the magma-filled fracture is:

$$Q_z^s = \frac{\Delta u^3 W}{12\mu}\left[\rho_m g - \frac{\partial p_e}{\partial z}\right] \tag{7}$$

where Δu is the aperture (opening) of the fracture (similar to a sheet thickness), W its width in a direction that is perpendicular to the flow direction (so that the fracture cross-sectional area perpendicular to the flow is $A = \Delta u W$, assuming that $W \gg \Delta u$), μ is the dynamic (absolute) viscosity and ρ_m the density of the magma (assumed constant), g is the acceleration due to gravity, and $\partial p_e / \partial z$ is the pressure gradient in the direction of the flow.

When the fracture and chamber walls are free to deform as magma is transported from the chamber, the weight of the rock above the chamber must be supported by its internal

pressure. Since the host-rock density ρ_r is different from the magma density ρ_m, a buoyancy term is added to the pressure gradient. Thus, for a vertical, elastic magma-filled fracture, Eq. (7) is rewritten in the form:

$$Q_z^e = \frac{\Delta u^3 W}{12\mu}\left[(\rho_r - \rho_m)g - \frac{\partial p_e}{\partial z}\right] \quad (8)$$

where Q_z^e is the volumetric rate of magma flow through a fracture in an elastic host rock.

Equations (7) and (8) apply for magma flow in vertical fractures such as many dykes. For inclined sheets, however, Eqs. (7) and (8) must be modified to account for the sheet dip α (Fig. 17). The dip dimension of the sheet, L, is the linear distance from the point of rupture of the magma chamber to the surface (Fig. 17). The volumetric rate Q_L^S of fluid flow along a self-supporting, inclined, magma-filled fracture, from Eq. (7) is then:

$$Q_L^s = \frac{\Delta u^3 W}{12\mu}\left[\rho_m g \sin\alpha - \frac{\partial p_e}{\partial L}\right] \quad (9)$$

By analogy with Eq. (8) , an inclined, elastic magma-filled fracture has a volumetric flow rate Q_L^e of:

$$Q_L^e = \frac{\Delta u^3 W}{12\mu}\left[(\rho_r - \rho_m)g \sin\alpha - \frac{\partial p_e}{\partial L}\right] \quad (10)$$

Equations (7) and (8) are special cases (with the dip $\alpha=90^\circ$ and thus $\sin\alpha=1$) of Eqs. (9) and (10). Similarly, flow of magma along a horizontal fracture, a sill, is a special case of Eqs. (9) and (10), where the dip $\alpha=0^\circ$ and thus $\sin\alpha=0$, and the first term in the brackets drops out. For a magma-filled fracture in the horizontal xy-plane, the width W being measured along the y-axis and the length L measured along the x-axis, we may substitute x for L and obtain, from Eqs. (9) and (10), the volumetric magma flow rate Q_x as:

$$Q_x = -\frac{\Delta u^3 W}{12\mu}\frac{\partial p_e}{\partial x} \quad (11)$$

so that the only pressure driving magma flow through the horizontal fracture is the excess pressure p_e (or the overpressure, in case the sill is fed by a vertical dyke) before the initiation of the sill.

Magma flow in feeder dykes—application

The aim of the numerical examples below is to show how the analytical formulas derived in the previous section can be used to understand some aspects of magma transport in sheet intrusions, with application to volcanic systems and central volcanoes (stratovolcanoes and calderas) in Iceland.

Consider a local sheet of thickness 0.5 m, an outcrop length/thickness ratio 1,000, and thus an outcrop length of 500 m. In Eqs. (7)–(11) we thus substitute 0.5 m for the aperture Δu, and 500 m for the length W. We use the typical tholeiite basalt viscosity of 100 Pa s (Murase and McBirney 1973), and density of 2,650 kg m^{-3} (Williams and McBirney 1979). The acceleration due to gravity is g=9.8 m s^{-2}, and the excess magmatic pressure in the chamber before rupture is $p_e=T_0$=3 MPa (equal to a typical in situ tensile strength of rocks). We assume that this excess pressure has the potential to drive the magma in a sheet intrusion from the top region of a typical shallow magma chamber in Iceland up to the surface of its central volcano, a vertical distance between 1,500 m and 2,500 m. For an average vertical depth of 2,000 m, it follows that the vertical pressure gradient is $\partial p_e/\partial z=-1{,}500$ Pa m^{-1}.

Substituting these values into Eq. (7), the volumetric flow rate through a vertical sheet in a rigid host rock is $Q_z^s \approx 1.4\times10^3\, m^3\, s^{-1}$. For the same values of magma density, viscosity and aperture and outcrop length of a sheet intrusion, and taking the average host-density for the uppermost 2 km of the crust in Iceland as 2,540 kg m^{-3}, then from Eq. (8) we get $Q_z^e \approx 22\ m^3\ s^{-1}$. The former value, for a fracture in a rigid host rock, is thus more than 60 times greater than that for a magma-transporting fracture in an elastic host rock, a difference largely due to negative buoyancy of a dense magma propagating through a low-density, elastic host rock.

Consider next the effect of sheet dip on magma transport. If the central volcano to which the sheet supplies magma is essentially flat, as is common in collapse calderas (Fig. 17), the linear distance of magma transport along an inclined sheet, L, is normally considerably longer than the shortest vertical distance, z, to the surface. If, however, the volcano forms a large topographic high such as a major stratovolcano, so that the elevation difference is several hundred metres or more, L may be similar to or even smaller than z. The difference between these distances thus depends on the topography of the central volcano, the geometry of the source chamber - which may ideally be cylindrical, spherical, prolate ellipsoidal, oblate ellipsoidal, or sill-like - and on the dip of the sheet that transports the magma. Both collapse calderas and stratovolcanoes exist in the volcanic zones of Iceland; the elevation difference between the marginal and central parts of the calderas is normally small, but may reach 1–2 km for the stratovolcanoes (Saemundsson 1978; Thorarinsson and Saemundsson 1979).

The condition $L=z$ is presumably appropriate for many stratovolcanoes. For brevity, we consider here only a magma-transporting fracture in an elastic host rock, using Eq. (10) and taking the magma density and viscosity, host-rock density and size of fracture to be the same as in the example above. The average dip of inclined sheets in Iceland is around $\alpha=60^\circ$. Then $\sin 60^\circ\approx0.87$ and Eq. (10) yields $Q_z^e \approx 19\ m^3 s^{-1}$. This value differs little from the earlier value, suggesting that for steeply dipping feeder sheets the assumption of their being vertical is reasonable when estimating magmatic flow (effusion) rates. Many shallow dipping sheets, however, have $\alpha=30^\circ$ (Figs. 5, 7, 14 and 15). Then $\sin 30^\circ=0.5$ and Eq. (10) gives $Q_z^e \approx 11\,\mathrm{m}^3\,\mathrm{s}^{-1}$, or half the value for the vertical sheet. Thus, for shallow

dipping feeder sheets, the assumption of their being vertical can lead to significant errors in estimating their potential for transporting magma to the surface of a central volcano.

For a flat central volcano, both the sheet dip and the geometry of the source chamber contribute to making $L>z$. Consider a sheet of dip α being injected from a roughly spherical magma chamber at a depth of x metres below the top of the chamber (Fig. 17). If L and z are in metres, then from trigonometry we have:

$$L = \frac{z + x}{\sin \alpha} \tag{12}$$

Consider, for example, a sheet dipping at α=60° being injected at depth x=500 m below the top of the chamber. Both these values would be expected to be common in local sheet swarms injected from roughly spherical chambers with a radius of 1–2 km (Gudmundsson 1998). Earlier, z was taken as 2 km, in which case Eq. (12) would give L as ~2.9 km. The average host rock density for the uppermost 2.5 km of the crust is 2,560 kg m^{-3}. Using this value for ρ_r, 2,900 m for L, so that the gradient $\partial p_e/\partial L$=−1,030 Pa m$^{-1,}$ and other values as in the example above, Eq. (10) gives $Q_z^e \approx 7.9\ m^3\ s^{-1}$. This volumetric flow rate is only around 40% of the value ($Q_z^e \approx 19\ m^3 s^{-1}$) obtained when the effect of sheet dip on L and the associated gradient $\partial p_e/\partial L$ was ignored.

Discussion

The models proposed in this paper indicate that one reason why so many periods of unrest in stratovolcanoes (with sheet injections) do not result in volcanic eruptions is that most sheet intrusions from magma chambers become arrested on their way to the surface. It is proposed that the arrest of sheet intrusions is primarily controlled by local variations in the stress field of the volcano. In this model, local variations in the stress field that contribute to sheet arrest are most commonly attributable to either stress barriers or mechanical anisotropy of the layers that make up the volcano. In stress barriers, the local stress field is unfavourable to the propagation of the particular type of sheet intrusion. For a vertical dyke, a stress barrier is a layer where the horizontal compressive stress perpendicular to the dyke is so high as to arrest the dyke tip (Figs. 1, 3, 12 and 13). Rock anisotropy includes contacts, joints and other discontinuities at which the sheet intrusion becomes arrested (Figs. 2 and 4). Most stress barriers are related to abrupt changes in stiffness, such as are common at contacts between different rock types (Figs. 9, 10, 15). It follows that stress barriers and anisotropy commonly operate together in arresting the tips of sheet intrusions.

The models explain, first, why the tips of many sheet intrusions become arrested at sharp contacts, at joints, or other discontinuities that traverse the potential pathway of the intrusion. Commonly, intrusions that terminate at these discontinuities have broad or even blunt tips (Fig. 2), suggesting that stress changes at the discontinuities are the main reason for the sheet arrest (Figs. 9, 10 and 15). Second, the models explain why, in vertical and horizontal sections, many sheet intrusions taper away within essentially homogeneous rock layers (Fig. 1; Gudmundsson 1995a, b). The general shape of these intrusions on approaching their tips indicates that they entered stress barriers (Figs. 12 and 13). In this case, the barrier is often due to decrease in intensity of the (relative or absolute) tensile stress with increasing distance from the magma chamber [Fig. 8; Eqs. (5) and, (6)].

Whether a sheet intrusion stops its extension at a weak contact, or propagates laterally along the contact as a sill, depends on several parameters. These include (1) the anisotropy of the in situ tensile strength in general, and that of the contact in particular, (2) the local stress field, and (3) the overpressure gradient. In Iceland, there are sheet intrusions that reach a contact between lava flows, follow the contact horizontally for several metres or more, and then continue their propagation up from the contact (Fig. 18). Normally, dykes become offset laterally on meeting sharp contacts in a lava pile. For some offset dykes, there are no clear connections across the contact between the subvertical segments; for other dykes, there are thin, igneous veins connecting the segments (Gudmundsson 1995a, b).

The effects of a horizontal discontinuity such as a weak or open contact, a joint or a fault on the vertical propagation of a dyke may exceed those of changes in Young's modulus. When a horizontal discontinuity such as a weak contact between layers is approached by the tip of a vertically propagating dyke, or any type of fluid-driven fracture (hydrofracture), the discontinuity tends to open up (Gudmundsson et al. 2002). An open discontinuity is a very effective stopper of fractures propagating perpendicular to the discontinuity. This mechanism of crack arrest is commonly referred to as the Cook-Gordon debounding mechanism; it applies in general to weak interfaces in the potential pathway of any type of fracture (Atkins and Mai 1985).

Fig. 18 Inclined sheet in the Pleistocene lava pile in Southwest Iceland (cf. Forslund and Gudmundsson 1991). The sheet, ~0.5–1 m thick, reaches the contact between the basaltic lava flow on the top and the scoria layer below, following the contact for several metres until it continues its propagation upwards in the pile

The Cook-Gordon mechanism may be partly responsible for the arrest of many dykes (Figs. 2 and 4). Also, sheet intrusions are commonly observed to follow the opened contact between layers for a while and then continue their propagation upwards in a lava pile (Fig. 18). In these cases, the sheet need not be, and seldom is, perpendicular to the minimum compressive stress while propagating along the horizontal contact. But the sheet follows the contact along part of its pathway because the tensile strength across the contact presumably became zero when it was opened by the sheet tip. Discontinuities and other crack stoppers commonly give rise to T-shaped fractures (Gudmundsson et al. 2002). The magma may then continue to flow laterally, as a sill, and perhaps renew its vertical or inclined propagation as a dyke or sheet further along the contact. Weak contacts and joints are presumably one of the most common reasons for offset sheet intrusions. Alternatively, depending on the magma overpressure, host-rock stresses and mechanical properties, a dyke may stop altogether at a contact (Fig. 2). A strong contrast in Young's moduli, or a strong stress contrast at the contact, for example, would commonly lead to the development of a T-shaped fracture (Gudmundsson et al. 2002).

In the models of magma flow presented by Eqs. (7)–(11) there are several simplifications in order to make the models mathematically tractable. For example, the effect of the differential stress $\sigma_d = \sigma_1 - \sigma_3$ is not included, but the plan is to do so in a future publication. Also, the excess magmatic pressure p_e, which is the primary driving pressure of flow through inclined basaltic sheets, is assumed constant, whereas it normally declines rapidly during the early stages of an eruption. After the rapid initial decline, however, the volumetric eruption rate normally settles to an approximately constant value for a considerable time. For example, apart from the beginning phase, much of the volumetric magma flow rate during the Hekla 1991 eruption was between 2 and 20 $m^3\ s^{-1}$ (Fig. 19). This is similar to the values for the 500-m-long sheet in an elastic host rock discussed above, where, depending on the sheet dip and magma-chamber geometry, Q_z^e ranged between 7.9 $m^3\ s^{-1}$ and 22 $m^3\ s^{-1}$. This suggests that the sheet intrusion transporting magma during most of the 1991 Hekla eruption may have had an opening of around half a metre and a length of several hundred metres.

There are, however, sometimes abrupt increases in volumetric flow rates during eruptions where the rate is otherwise gently declining (Fig. 19). These are likely to relate to two principal causes: either additional magma received by the source chamber, or changes in the geometry (particularly an increase in the opening) of the feeder sheet or dyke. There is no evidence of the Hekla chamber receiving significant volumes of new magma during the 1991 eruption, but it is known that the geometry and location of the eruptive vents (and by implication, the feeder sheet) changed during the course of the eruption (Gudmundsson et al. 1992). Such increases in volumetric magma flow rates, however, are normally short-lived; unless there is much magma added to the source chamber, its excess pressure, and thus the driving pressure of the feeder sheet, continues to decline during the course of the eruption.

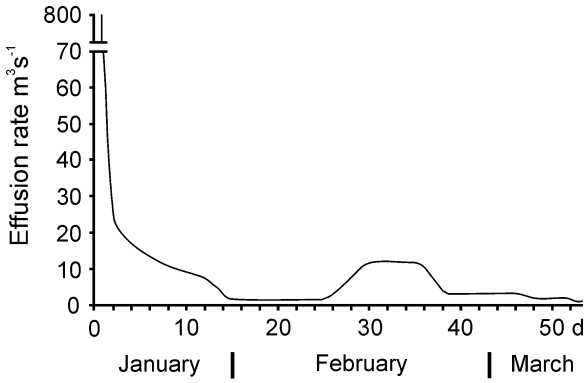

Fig. 19 Variation in effusion rate during the 1991 eruption of Hekla (Iceland), with the number of days since the start of the eruption on the horizontal axis and the volumetric magma flow rate on the vertical axis. Modified from Gudmundsson et al. (1992)

The models on sheet emplacement and magma transport presented in this paper need to be improved and refined in a future work. Nevertheless, at this stage of their development they are able to account for many measurable parameters associated with sheets and dykes and, in addition, make predictions that are quantitative and testable. These predictions include the following. (1) Most sheets and dykes become arrested, primarily due to discontinuities and stress barriers that traverse their potential propagation pathways. (2) A necessary condition for sheets and dykes to reach the surface is stress-field homogenisation in the crust above the source magma chamber. (3) Shallow-dipping sheets normally transport less magma in unit time than equally sized, vertical sheets and dykes.

Acknowledgements This work was supported through a grant from the European Commission (EVG1-CT-2002-00073 PREPARED), several grants from the Norway Research Council, as well as a PhD grant from Statoil (to A. Gudmundsson) for S. L. Brenner. We thank the Bulletin Volcanology reviewers for helpful comments

References

Afrouz AA (1992) Practical handbook of rock mass classification systems and modes of ground failure. CRC Press, London, pp 1–195

Amadei B, Stephansson O (1997) Rock stress and its measurement. Chapman & Hall, London, pp 1–490

Anderson EM (1936) The dynamics of formation of cone sheets, ring dykes and cauldron subsidence. Proc R Soc Edinburgh 56:128–163

Atkins AG, Mai YW (1985) Elastic and plastic fracture. Horwood, Chichester, pp 1–817

BEASY (1991) The boundary element analysis system user guide. Computational Mechanics, Boston

Bell FG (2000) Engineering properties of rocks, 4th edn. Blackwell, Oxford, pp 1–482

Benham PP, Crawford RJ, Armstrong CG (1996) Mechanics of engineering materials. Prentice Hall, New Jersey, pp 1–644

Billings MP (1972) Structural geology, 3rd edn. Prentice-Hall, New Jersey, pp 1–606

Bonafede M, Rivalta E (1999) The tensile dislocation problem in a layered elastic medium. Geophys J Int 136:341–356
Brebbia CA, Dominguez J (1992) Boundary elements: an introduction course. Computational Mechanics, Boston, pp 1–314
Brenner SL, Gudmundsson A (2002) Permeability development during hydrofracture propagation in layered reservoirs. Geol Surv Norway Bull 439:71–77
Delaney PT, McTigue DF (1994) Volume of magma accumulation or withdrawal estimated from surface uplift or subsidence, with application to the 1960 collapse of Kilauea Volcano. Bull Volcanol 56:417–424
Forslund T, Gudmundsson A (1991) Crustal spreading due to dikes and faults in southwest Iceland. J Struct Geol 13:443–457
Gautneb H, Gudmundsson A, Oskarsson N (1989) Structure, petrochemistry, and evolution of a sheet swarm in an Icelandic central volcano. Geol Mag 126:659–673
Goodman RE (1989) Introduction to rock mechanics, 2nd edn. Wiley, New York, pp 1–562
Gudmundsson A (1995a) The geometry and growth of dykes. In: Baer G, Heimann A (eds) Physics and chemistry of dykes. Balkema, Rotterdam, pp 23–34
Gudmundsson A (1995b) Infrastructure and mechanics of volcanic systems in Iceland. J Volcanol Geotherm Res 64:1–22
Gudmundsson A (1998) Magma chambers modeled as cavities explain the formation of rift zone central volcanoes and their eruption and intrusion statistics. J Geophys Res 103:7401–7412
Gudmundsson A (2002) Emplacement and arrest of sheets and dykes in central volcanoes. J Volcanol Geotherm Res 116:279–298
Gudmundsson A, Bergerat F, Angelier J (1996) Off-rift and rift-zone palaeostresses in northwest Iceland. Tectonophys 255:211–228
Gudmundsson A, Fjeldskaar I, Brenner SL (2002) Propagation pathways and fluid transport of hydrofractures in jointed and layered rocks in geothermal fields. J Volcanol Geotherm Res 116:257–278
Gudmundsson A, Oskarsson N, Gronvold K, Saemundsson K, Sigurdsson O, Stefansson R, Gislason SR, Einarsson P, Brandsdottir B, Larsen G, Johannesson H, Thordarson T (1992) The 1991 Hekla eruption. Bull Volcanol 54:238–246
Haimson BC, Rummel F (1982) Hydrofracturing stress measurements in the Iceland research drilling project drill hole at Reydarfjordur, Iceland. J Geophys Res 87:6631–6649
Hills ES (1972) Elements of structural geology, 2nd edn. Chapman and Hall, London, pp 1–502
Jing L, Hudson JA (2002) Numerical methods in rock mechanics. Int J Rock Mech Min Sci 39:409–427
Klausen MB (1999) Structure of rift-related igneous systems and associated crustal flexures. PhD thesis, University of Copenhagen
Klausen MB (2004) Geometry and mode of emplacement of the Thverartindur cone sheet swarm, SE Iceland. J Volcanol Geotherm Res 138:185–204
Lamb H (1932) Hydrodynamics, 6th edn. Cambridge University Press, Cambridge, pp 1–738
Lister JR, Keer RC (1991) Fluid-mechanical models of crack propagation and their application to magma transport in dikes. J Geophys Res 96:10,049–10,077
Logan DL (2002) A first course in the finite element method. Brooks/Cole, Pacific Grove, pp 1–696
Marinoni LB, Gudmundsson A (2000) Dykes, faults and palaeostresses in the Teno and Anaga massifs of Tenerife (Canary Islands). J Volcanol Geotherm Res 103:83–103
McTigue DF (1987) Elastic stress and deformation near a finite spherical magma body: resolution of the point source paradox. J Geophys Res 92:12,931–12,940
Milne-Thompson LM (1996) Theoretical hydrodynamics, 5th edn. Dover, New York, pp 1–744
Mogi K (1958) Relations between eruptions of various volcanoes and the deformations of the ground surfaces around them. Bull Earthquake Res Inst 36:99–134
Murase T, McBirney AR (1973) Properties of some common igneous rocks and their melts at high temperatures. Bull Geol Soc Am 84:3563–3592
Pallister JS (1981) Structure of the sheeted dike complex of the Samail ophiolite near Ibra, Oman. J Geophys Res 86:2661–2672
Priest SD (1993) Discontinuity analysis for rock engineering. Chapman & Hall, London, pp 1–473
Rubin AM (1995) Propagation of magma-filled cracks. Ann Rev Earth Planet Sci 23:287–336
Saada AS (1983) Elasticity: theory and applications. Krieger, Malabar, Florida, pp 1–643
Saemundsson K (1978) Fissure swarms and central volcanoes of the neovolcanic zones of Iceland. In: Bowes DR, Leake BE (eds) Crustal evolution in northwestern Britain and adjacent regions. Geol J Spec Issue 10:415–432
Savin GN (1961) Stress concentration around holes. Pergamon, London, pp 1–430
Schirnick C, van den Bogaard P, Schmincke HU (1999) Cone sheet formation and intrusive growth of an oceanic island – The Miocene Tejeda complex on Gran Canaria (Canary Islands). Geology 27:207–210
Schultz RA (1995) Limits of strength and deformation properties of jointed basaltic rock masses. Rock Mech Rock Eng 28:1–15
Spence DA, Sharp PW, Turcotte DL (1987) Buoyancy-driven crack propagation: a mechanism for magma migration. J Fluid Mech 174:135–153
Thorarinsson S, Saemundsson K (1979) Volcanic activity in historical time. Jokull 29:29–32
Walker GPL (1992) "Coherent intrusive complexes" in large basaltic volcanoes—a new structural model. J Volcanol Geotherm Res 50:41–54
Walker GPL (1999) Volcanic rift zones and their intrusion swarms. J Volcanol Geotherm Res 94:21–34
Williams H, McBirney AR (1979) Volcanology. Freeman, San Francisco, pp 1–397
Zienkiewicz OC (1977) The finite element method, 3rd edn. McGraw-Hill, London, pp 1–787